COMMUNICATION

Check for updates

Crystalline borophene quantum dots and their derivative boron nanospheres†

Huiqi Wang, ‡*[a] Duo An,‡[a] Mei Wang,[a] Liwen Sun,[a] Ying Li,[a] Hairu Li,[a] Ning Li, [a] Shengliang Hu *[a] and Yan-Bing He *[b]

Crystalline borophene quantum dots with two-photo fluorescence and their derivative boron nanospheres with hydrazine hydrate-dependent photoluminescence properties were prepared by an efficient high-power sonication method combined with chemical exfoliation and a one-step chemical coupling strategy, respectively. This work would extend the practical lighting applications of B-rich nanomaterials.

Following the carbon science development, various low-dimensional boron nanostructures, such as all-boron clusters,[1,2] nanowires,[3] nanotubes,[4,5] fullerenes,[6] and two-dimensional (2D) nanosheets,[7,8] have been reported experimentally and theoretically in the past two decades. Since the experimental realization of borophene,[9] synthetic boron nanomaterials have been prompting extensive research studies due to their structural complexity and exceptional physical and chemical properties, e.g., superhardness, superconductivity, high carrier mobility, and neutron-capturing capacity.[10–12] However, boron differs from its neighbor, carbon, in the periodic table, and none of the pure boron materials exhibit 2D layered structures due to its severe electron-deficiency nature with multicenter features. Consequently, it was difficult to prepare representative borophenes by a simple exfoliation process, until Vinu et al.[13] reported recently the discovery of a scalable and liquid-phase synthesis of borophene sheets via sonochemical exfoliation, and the small sheet-sized borophene can be fabricated by using water and isopropyl alcohol as liquid-phase exfoliation solvents. The ultrasmall boron nanoparticles are likely to be prepared by exfoliating the bulk boron through physical and chemical technologies. As expected, boron quantum dots proposed by Tai et al.,[14] a new cousin of carbon

quantum dots, were synthesized successfully, provoking the growing passion for zero-dimensional crystalline boron nanomaterials.

As extraordinary zero-dimensional materials, carbon quantum dots (CQDs) exhibit good chemical, electrical, and photoluminescence (PL) characteristics, and offer great potential in drug delivery, sensing, bioimaging, and diagnostic applications. Inspired by the CQDs,[15] fabrication strategies, e.g., "bottom-up" and "top-down", are expected to synthesize the boron-based quantum dots (BQDs). In the bottom-up process, a series of small molecules were combined and assembled into BQDs through chemical reactions, while the top-down approach begins with the exfoliation of bulky boron-rich precursors, such as boron powders, boron fibers, boron nanotubes, and borophenes. Generally, the top-down methods have advantages of abundant raw materials and mass production.[15] To date, both sonication-assisted liquid-phase exfoliation and chemical exfoliation have been shown to be effective for the production of large quantities of 0D and 2D materials.[16–18] Compared with chemical exfoliation, sonication-assisted liquid-phase exfoliation is expected to be a more promising strategy to prepare BQDs. Recently, Tai et al.[14] have synthesized the crystalline BQDs by the probe ultrasonic procedure using the expanded boron powders as the raw material in a highly polar organic solvent. The as-synthesized BQDs are approximately 2.5 nm in lateral size and 2.8 nm in thickness and exhibit strong quantum confinement effects, named zero-dimensional QDs. To date, the borophene QDs (B-QDs), which resemble those of graphene QDs (G-QDs), are rarely reported experimentally. As is well-known, G-QDs were endowed with excellent properties of graphene, and their quantum confinement and surface/edge effects benefiting from their lateral dimension of ≤10 nm and thickness of ≤2 nm give two-dimensional QDs with superior physicochemical properties, such as high quantum yield, adjustable band gap, size-dependent photoluminescence, a mass of active sites, and better dispersibility.[15,19,20] As a result, they have many broad application prospects in optoelectronics, catalysis, sensing, bioimaging, and cancer therapy. Therefore, tireless efforts are urgently needed to exploit synthetic B-QDs.

Herein, we propose a synthesis strategy towards a new class of quantum dots, i.e., B-QDs obtained by low-temperature

[a] School of Energy and Power Engineering & School of Materials Science and Engineering, North University of China, Taiyuan 030051, China.
E-mail: hqiwang@nuc.edu.cn, hsliang@yeah.net
[b] Shenzhen Geim Graphene Center, Tsinghua Shenzhen International Graduate School, Tsinghua University, Shenzhen, 518055, P. R. China.
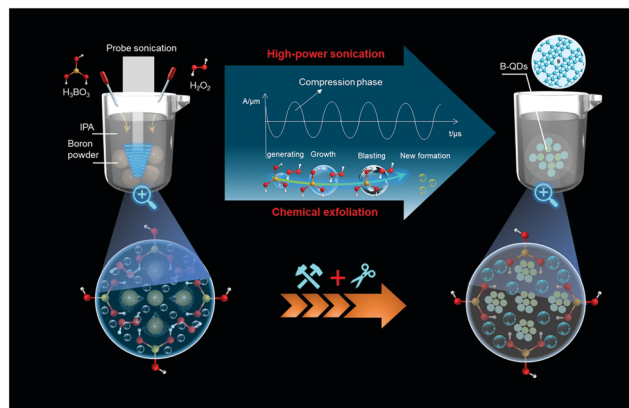E-mail: he.yanbing@sz.tsinghua.edu.cn

Fig. 1 Schematic illustration of the synthetic procedure for B-QDs.

liquid-phase exfoliation. The prepared B-QDs are monodispersed with a narrow size distribution (with an average size of 3.5 nm), excellent dispersibility, high stability in IPA solution, and two-photo fluorescence. Interestingly, the obtained B-QDs can be transformed into boron nanospheres through coupling strategy by hydrazine hydrate (HHA, Fig. S1, ESI†), and these nanospheres exhibit HHA-dependent PL properties.

The novel B-QDs were prepared by the probe sonication-assisted liquid-phase exfoliation method in a low-temperature environment (Fig. 1). In the experimental setup, the liquid-phase environment consists of boric acid, hydrogen peroxide and IPA. Boric acid is regarded as an important factor for fabricating the B-QDs. The results of TEM images (Fig. S2, ESI†) show that the B-QDs were unable to be prepared in the IPA solution without boric acid. The addition of hydrogen peroxide was doubled to create a larger liquid–gas interface to peel the boron particles, and thus form a mass of B-QDs with a smaller size and a narrower size distribution. Importantly, owing to the cavitation effect, vacuum bubbles were produced under high-power probe ultrasonic treatment. The ultrahigh shock waves produced by the implosive collapse of these bubbles crushed the boron particles into pieces.[13]

The TEM image (Fig. 2a) reveals that B-QDs are well-dispersed and have an average size of approximately 3.5 nm. The atomic force microscopy (AFM) image (Fig. 2b) shows a typical topographic height between 1 and 2 nm that indicates a 1–3 layered borophene. The high-resolution TEM (HR-TEM) images (Fig. 2c and d) show that B-QDs have a superlattice structure with an interplanar distance of about 0.22 nm, corresponding to the (404) lattice planes of β-rhombohedral boron. The corresponding fast Fourier transform (FFT) diffraction patterns (Fig. 2e) of the representative individual B-QDs further demonstrate the crystalline nature, but these observations of distinct features in FFT patterns seems to result from the two boron phases, which are similar to the most well-known borophene structure with β_{12} and χ_3 phases.[13,21] The high-angle annular dark-field (HAADF) scanning TEM (STEM) image of numerous B-QDs (Fig. 2f) shows a clear dot-like structure. The energy-dispersive X-ray spectroscopy (EDX) elemental
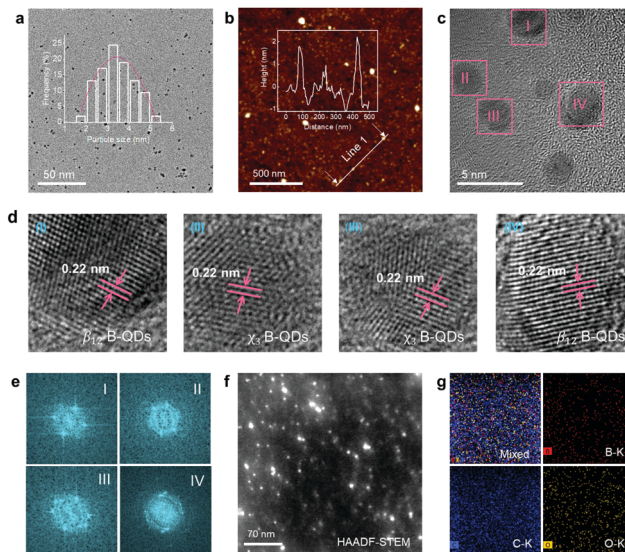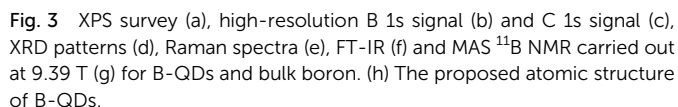

Fig. 2 Morphology and structure of B-QDs. (a) TEM image. The inset in (a) shows the size distribution of B-QDs. (b) AFM image. The inset in (b) shows the topographic height corresponding to the white line zone; (c and d) HR-TEM image. The white circles in (b) mark the locations of single B-QDs. (e) FFT of the HR-TEM image in (c). HAADF-STEM image (f) and the corresponding EDX mapping images (g) of the mixed picture, B, C and O.

mappings (Fig. 2g) of B, C and O correspond to the area shown in Fig. 2f. The existence of C is likely due to the surface contamination that occurs during the exposure to air atmosphere and the exfoliating solvent.
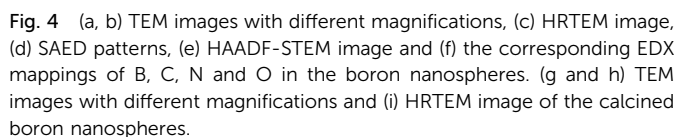
Furthermore, the XPS survey (Fig. 3a) suggests the existence of B, C and O elements in the B-QDs. Notably, there is an obvious change in the atomic ratios of B and O elements for B-QDs compared to that for the bulk boron (Fig. S3, ESI†), indicating that fresh B-QDs were highly unstable and easily oxidized. The high-resolution B 1s signal of B-QDs (Fig. 3b) is fitted into three peaks at 186.8 eV, 188.5 eV and 192.2 eV. In comparison with the bulk boron, the three peaks of B-QDs were red-shifted, confirming the successful fabrication of B-QDs after the probe sonication-assisted liquid-phase exfoliation of the bulk boron, which is similar to the previous results of BQDs.[14,22] The peaks at 186.8 eV and 188.5 eV are attributed to the B–B bonds.[22,23] The component at 188.5 eV is possibly related to the coordinatively unsaturated boron atoms at the surface of B-QDs due to the distorted edge-effect.[22] The peak at 192.2 eV is mainly ascribed to the formation of B_2O_3.[21,22] The high-resolution C 1s signals (Fig. 3c) for both B-QDs and bulk boron can be deconvoluted into three peaks at 284.8 eV, 286.3 eV and 288.7 eV, which may be due to the C–C, C–O, and C=O bonds, respectively. However, no C–B signal exists, demonstrating that a shell consisted of C and O elements formed on the edges of B-QDs. Powder XRD patterns (Fig. 3d) of the as-collected B-QDs disclose the crystal structure, which can be indexed to the β-rhombohedral boron (PDF #80-0323),[22] indicating that the B-QDs still have a crystalline boron structure and are derived from the bulk boron. This result is in good agreement with the structural parameters obtained by the HR-TEM images.

Fig. 3 XPS survey (a), high-resolution B 1s signal (b) and C 1s signal (c), XRD patterns (d), Raman spectra (e), FT-IR (f) and MAS ^{11}B NMR carried out at 9.39 T (g) for B-QDs and bulk boron. (h) The proposed atomic structure of B-QDs.
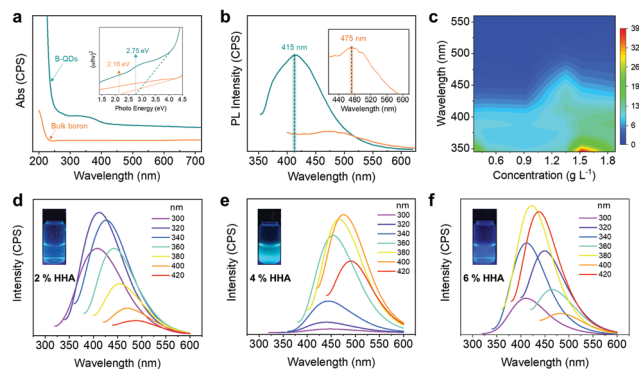
The complicated structural and chemical features of B-QDs with different boron polymorphs were characterized by combining Raman spectra (Fig. 3e), FT-IR spectra (Fig. 3f), and MAS ^{11}B-NMR spectra (Fig. 3g). The different boron polymorphs can be distinguished by their distinct Raman spectra.[24,25] Raman spectrum of the B-QDs (Fig. 3e) in the spectral range of 200–1200 cm^{-1} exhibits two sharp peaks at 576 and 1058 cm^{-1}, attributed to the two breathing modes of β_{12} phase in the B-QDs.[24] The two peaks can be attributed to the intra-icosahedral vibrations located at 576 cm^{-1} (B_{3g}^1) and the two-center B–B bonds located at 1058 cm^{-1} (B_{1g}^1), respectively.[22,24,26] The other peaks at 409, 469 and 763 cm^{-1} were probably attributed to the vibration modes of the χ_3 phase in the B-QDs, which were attributed to B_g^1, B_g^1 (Y) and B_g^3, respectively.[24] These results verified the atomic structure of the B-QDs observed by the HR-TEM images (Fig. 2c and d), suggesting the presence of β_{12} and χ_3 phases in the B-QDs in this work (Fig. 3h). It should be mentioned that the peaks at 1363 and 1617 cm^{-1} may originate from the carbon lattice vibration modes,[27] indicating that the shell formed on the edges of the B-QDs contains a large number of carbon species. On the basis of XPS results, the bonding environments of boron in the B-QDs were fully clarified by combining FT-IR and MAS ^{11}B-NMR. The FT-IR spectrum of the B-QDs (Fig. 3f) shows two characteristic peaks centred at 1364 and 3415 cm^{-1} attributed to B–O and B–OH, respectively.[13] This result indicates that partial oxidation of boron occurred on the edges of the B-QDs. All the left peaks in the FT-IR spectrum (Fig. 3e) were attributed to B–B vibrations.[13,22] The chemical shift and line shape in the MAS ^{11}B-NMR spectra may be directly associated with the coordination environment of boron.[28–30] The chemical shift at 0.62 ppm is attributed to B–B icosahedra,[28] and the chemical shift at 36.4 ppm arises from the B–B bonds in the triangular lattice with periodic hole arrays. The

other chemical shifts at <0 ppm may be ascribed to the tetrahedral B–O groups.[28,29]

The morphologies of the derivative boron nanospheres (DBS) were observed by TEM and SEM. Fig. 4a and Fig. S4 (ESI†) clearly reveal that the obtained DBS have a spherical shape with a diameter of 150 nm. The TEM image shown in Fig. 4b displays the microstructural feature of DBS that the nanospheres consist of ultrasmall B-QD particles and some cavities. The appearance of these cavities maybe due to the removal of organic components caused by the electron beam irradiation in the course of TEM measurements. The HR-TEM image in Fig. 4c shows the interconnected B-QD particles with a lattice fringe of 0.46 nm, which corresponds to the (021) lattice planes of boron. The selected area electron diffraction pattern (SAED) of DBS shown in Fig. 4d depicts a spotty ring pattern with mild polycrystalline nature, which can be clearly attributed to the diffractions of the (021) boron lattice planes. The HAADF-STEM image shown in Fig. 4e confirms the inner structural features as shown in Fig. 4b. The EDX mappings reveal the uniform distribution of B, C, N, and O elements. The existence of the N element is caused by the hydrazine hydrate. This result suggests that hydrazine hydrate coupled with numerous B-QDs to be assembled into the spherical particles. Nevertheless, after calcining the DBS at 500 °C, the diameter of the obtained DBS particles is reduced to around 30 nm owing to the removal of hydrazine hydrate, forming the amorphous boron. The TEM images shown in Fig. 4g and h confirm the reduced diameter and almost the vanishing of the scattered B-QDs. The SAED pattern shown in the inset of Fig. 4h displays a cloudy diffraction ring attributed to its amorphous nature. The HR-TEM image shown in Fig. 4i further reveals the disordered structure

Fig. 4 (a, b) TEM images with different magnifications, (c) HRTEM image, (d) SAED patterns, (e) HAADF-STEM image and (f) the corresponding EDX mappings of B, C, N and O in the boron nanospheres. (g and h) TEM images with different magnifications and (i) HRTEM image of the calcined boron nanospheres.

Fig. 5 Optical properties. (a) UV-vis spectra. (b) PL spectra excited by a 325 nm laser. (c) 3D mapping picture of B-QD concentration-dependent fluorescence excitation. (d–f) PL spectra of the DBS with different HHA concentrations excited at various wavelengths. The insets show the digital image under UV lamp irradiation of 365 nm.

of the boron occupied, and only a few crystalline B-QD nanoparticles existed in the calcined boron nanospheres.

The optical properties of the obtained B-QDs and DBS were investigated by ultraviolet-visible (UV/Vis) absorption and photoluminescence (PL) spectroscopies. For the B-QDs, the UV-vis spectrum shown in Fig. 5a suggests that the B-QDs are semiconducting and the corresponding optical bandgap (E_g) was calculated to be 2.75 eV according to $(\alpha h\upsilon)^2 = h\upsilon - E_g$, where α is the absorption coefficient and $h\upsilon$ is the photon energy. This value is much higher than that of the bulk boron (2.16 eV), which is attributed to the strong quantum-confinement effect in the B-QDs. The B-QDs, exhibiting a light black phase, can be dispersed in the IPA solution. The Tyndall effect can be observed, indicating the colloidal nature of B-QD dispersion. The B-QD dispersion is quite stable at room temperature for 60 days without any obvious aggregation and precipitation (Fig. S5a, ESI†). A characteristic peak in the PL spectrum shown in Fig. 5b was located at about 415 nm (with a photon energy of 2.75 eV) for the B-QDs and about 478 nm for the bulk boron (with a photon energy of 2.15 eV), which was in good agreement with the absorption spectrum. The obvious blue shift of 63 nm in the PL spectra may be due to the quantum size effect,[31] which is similar to the graphene QDs with the ultrafine size and distorted edge-defects.[19] The B-QDs show two-photon fluorescence as well (Fig. 5c). Similar to the one-photon fluorescence, two emission peaks appear under 360 nm laser excitation (Fig. S5b and S6, ESI†). The optimal emission of B-QDs should be at 386 nm with a shoulder peak at 401 nm. With the decrease of the B-QD concentration to 1.35 g L^{-1}, the two peaks shift to 415 and 437 nm, respectively. The absorbance of B-QDs also decreases as the concentration reduces and two absorption peaks were detected at about 290 and 372 nm (Fig. S5c, ESI†). Moreover, the PL spectra of DBS shown in Fig. 5d–f suggest that the PL properties were dependent on the concentration of HHA. The DBS displays three colors under the visible light of 365 nm (the inset of Fig. 5d–f). Thus, this work would extend the practical lighting applications of B-based materials.

In conclusion, we have successfully prepared crystalline B-QDs through liquid-phase exfoliation using high-power sonication combined with chemical exfoliation. The as-prepared B-QDs are monodispersed with a narrow size distribution, excellent dispersibility, high stability in IPA solution, and two-photo fluorescence. The obtained B-QDs can be transformed into boron nanospheres through a one-step coupling strategy by means of hydrazine hydrate (HHA), and these nanospheres exhibit HHA-dependent PL properties. Currently, we are boosting further investigations on the applications of two-photon fluorescence of our B-QDs.

Conflicts of interest

There are no conflicts to declare.

Acknowledgements

Notes and references

1 W.-L. Li, Q. Chen, W.-J. Tian, H. Bai, Y.-F. Zhao, H.-S. Hu, J. Li, H.-J. Zhai, S.-D. Li and L.-S. Wang, *J. Am. Chem. Soc.*, 2014, **136**, 12257–12260.

2 X.-Y. Zhao, Q. Chen, H.-R. Li, Y.-W. Mu, H.-G. Lu and S.-D. Li, *Phys. Chem. Chem. Phys.*, 2017, **19**, 10998–11003.

3 Y. Zhang, F. Liu, C. Shen, T. Yang, J. Li, S. Deng, N. Xu and H. Gao, *Chinese Physics B*, 2016, **25**, 078101.

4 D. Ciuparu, R. F. Klie, Y. Zhu and L. Pfefferle, *J. Phys. Chem. B*, 2004, **108**, 3967–3969.

5 J. Kunstmann, V. Bezugly, H. Rabbel, M. H. Ruemmeli and G. Cuniberti, *Adv. Funct. Mater.*, 2014, **24**, 4127–4134.

6 H.-J. Zhai, Y.-F. Zhao, W.-L. Li, Q. Chen, H. Bai, H.-S. Hu, Z. A. Piazza, W.-J. Tian, H.-G. Lu, Y.-B. Wu, Y.-W. Mu, G.-F. Wei, Z.-P. Liu, J. Li, S.-D. Li and L.-S. Wang, *Nat. Chem.*, 2014, **6**, 727–731.

7 X. Wu, J. Dai, Y. Zhao, Z. Zhuo, J. Yang and X. C. Zeng, *ACS Nano*, 2012, **6**, 7443–7453.

8 B. Feng, J. Zhang, Q. Zhong, W. Li, S. Li, H. Li, P. Cheng, S. Meng, L. Chen and K. Wu, *Nat. Chem.*, 2016, **8**, 564–569.

9 A. J. Mannix, X.-F. Zhou, B. Kiraly, J. D. Wood, D. Alducin, B. D. Myers, X. Liu, B. L. Fisher, U. Santiago, J. R. Guest, M. J. Yacaman, A. Ponce, A. R. Oganov, M. C. Hersam and N. P. Guisinger, *Science*, 2015, **350**, 1513–1516.

10 X. Sun, X. Liu, J. Yin, J. Yu, Y. Li, Y. Hang, X. Zhou, M. Yu, J. Li, G. Tai and W. Guo, *Adv. Funct. Mater.*, 2017, **27**, 1603300.

11 G. Tai, T. Hu, Y. Zhou, X. Wang, J. Kong, T. Zeng, Y. You and Q. Wang, *Angew. Chem., Int. Ed.*, 2015, **54**, 15473–15477.

12 X. Wang, J. Liang, Q. You, J. Zhu, F. Fang, Y. Xiang and J. Song, *Angew. Chem., Int. Ed.*, 2020, **59**, 23559–23563.
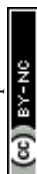
13 P. Ranjan, T. K. Sahu, R. Bhushan, S. S. Yamijala, D. J. Late, P. Kumar and A. Vinu, *Adv. Mater.*, 2019, **31**, 1900353.

14 J. Hao, G. Tai, J. Zhou, R. Wang, C. Hou and W. Guo, *ACS Appl. Mater. Interfaces*, 2020, **12**, 17669–17675.

15 J. Zhu, Y. Dong, S. Zhang and Z. Fan, *Acta Phys.-Chim. Sin.*, 2020, **36**, 1903052.

16 H. Li, L. Jing, W. Liu, J. Lin, R. Y. Tay, S. H. Tsang and E. H. T. Teo, *ACS Nano*, 2018, **12**, 1262–1272.

17 X. Wang, X. Yu, J. Song, W. Huang, Y. Xiang, X. Dai and H. Zhang, *Chem. Eng. J.*, 2021, **406**, 126876.

18 X. Wang, J. Song and J. Qu, *Angew. Chem., Int. Ed.*, 2019, **58**, 1574–1584.

19 S. Jeong, R. L. Pinals, B. Dharmadhikari, H. Song, A. Kalluri, D. Debnath, Q. Wu, M.-H. Ham, P. Patra and M. P. Landry, *Sci. Rep.*, 2020, **10**, 7074.

20 X. Wang, J. He, B. Zhou, Y. Zhang, J. Wu, R. Hu, L. Liu, J. Song and J. Qu, *Angew. Chem., Int. Ed.*, 2018, **57**, 8668–8673.

21 B. Feng, J. Zhang, Q. Zhong, W. Li, S. Li, H. Li, P. Cheng, S. Meng, L. Chen and K. Wu, *Nat. Chem.*, 2016, **8**, 564–569.

22 L. Wang, S.-M. Xu, S. Guan, X. Qu, G. I. N. Waterhouse, S. He and S. Zhou, *J. Mater. Chem. B*, 2020, **8**, 9881–9887.

23 T. T. Xu, J.-G. Zheng, N. Q. Wu, A. W. Nicholls, J. R. Roth, D. A. Dikin and R. S. Ruoff, *Nano Lett.*, 2004, **4**, 963–968.

24 S. Sheng, J.-B. Wu, X. Cong, Q. Zhong, W. Li, W. Hu, J. Gou, P. Cheng, P.-H. Tan, L. Chen and K. Wu, *ACS Nano*, 2019, **13**, 4133–4139.

25 H. Werheit, V. Filipov, U. Kuhlmann, U. Schwarz, M. Armbrüster, A. Leithe-Jasper, T. Tanaka, I. Higashi, T. Lundström, V. N. Gurin and M. M. Korsukova, *Sci. Technol. Adv. Mater.*, 2010, **11**, 023001.

26 Z. Wu, G. Tai, W. Shao, R. Wang and C. Hou, *Nanoscale*, 2020, **12**, 3787–3794.

27 H. Wang, Q. Guo, J. Yang, Z. Liu, Y. Zhao, J. Li, Z. Feng and L. Liu, *Carbon*, 2013, **56**, 296–308.

28 C. L. Turner, R. E. Taylor and R. B. Kaner, *J. Phys. Chem. C*, 2015, **119**, 13807–13813.

29 N. P. Stadie, E. Billeter, L. Piveteau, K. V. Kravchyk, M. Döbeli and M. V. Kovalenko, *Chem. Mater.*, 2017, **29**, 3211–3218.

30 H. Wang, Y. Li, Y. Wang, S. Hu and H. Hou, *J. Mater. Chem. A*, 2017, **5**, 2835–2843.

31 J.-H. Yang, J.-F. Gao, S.-L. Yong, X.-L. Ma and L.-J. Liu, *Rare Met.*, 2019, **38**, 1097–1104.